Development and lattice design of an ion-production ring for a beta-beam neutrino facility

Bachelor Thesis
Michaela Schaumann

RWTH Aachen University
Supervisor: Prof. Dr. Achim Stahl

CERN
European organization for nuclear research
Co-Supervisor: Dr. Elena Wildner

CERN-THESIS-2009-128
18/09/2009

Abstract

Neutrino beams can be produced by accelerating beta active ions which will decay in a race track accelerator ring to produce intense focused neutrino beams. The production of these radioactive isotopes need special technology. One idea [1] is to let a circulating low energy beam of ^7Li or ^6Li in a small production ring perform multiple traversals in a target to produce ^8Li and ^8B.
The lattice of this production ring has to satisfy conditions to permit the radioactive isotope production but also to permit ionization cooling of the circulating beam. The lattice should be flexible and have margins for further optimization.
This thesis describes the design of such a production ring lattice, having symmetry and flexibility. A simplified model of the wedge shaped target has been implemented, using results from Monte Carlo simulations [3], and is used as an element in the lattice to perform 6D tracking simulations of the cooling process. Tools for this simulation have been developed and tested.

14. September 2009

Contents

1 Introduction

1.1 Motivation

Based on Ray Davis's Homestake Experiment in the late 1960s, in which he observed a deficit in the flux of solar neutrinos using a chlorine-based detector, neutrino oscillation was discovered. A neutrino, created with a specific lepton flavour (electron, muon or tau), can later be measured with a different flavour. The probability of measuring the neutrino with a particular flavour varyies periodically while it propagates. Neutrino oscillation is of theoretical and experimental interest, because this phenomenon implies a non-zero neutrino mass, which is not part of the original standard model of particle physics.
Henceforward several techniques for the measurement of the effect of neutrino oscillation were built, but up to now it could not be completely investigated. Some important parameters for the description of this phenomenon are still not measured exactly.
In 1962 the Maki–Nakagawa–Sakata matrix (MNS matrix) was introduced to describe the phenomenon of neutrino oscillation. This matrix describes the mixing of the different neutrino flavours, like the CKM matrix do in the quark sector. As a result, the neutrino oscillation probability depends on three mixing angles, $\theta_{12}, \theta_{23}, \theta_{13}$, two mass differences, $\Delta m^2_{12}, \Delta m^2_{23}$, and a CP phase δ_{CP}. Additional phases are present in case neutrinos are Majorana particles, but they do not influence at all neutrino flavour oscillation.
The phase factor and θ_{13}, the mixing angle between the first and the third generation (electron and tau), are still unknown. Also the sign of the mass difference Δm^2_{32} is unknown.

There are three approaches, Neutrino factory, beta beams and superbeams, to produce a focused (anti-)neutrino beam. This beam will then be measured in a long or a short baseline experiment to investigate the neutrino oscillation and the missing parameters. In this thesis we will concentrate only on beta-beams.

1.1.1 Beta Beams

The basic idea of beta-beams is to produce radioactive ions by sending a proton beam or an ion beam onto a target designed for the creation of unstable nuclei, accelerate them and due to the beta-decay in long straight sections in the storage ring, a focused neutrino beam is obtained.

The major difficulty is to obtain enough radioactive ions to produce the required flux of neutrinos. The optimal decay time of the radioactive ion is $\sim 1\,s$, so that the produced nucleus can be extracted and accelerated without too much ion losses through decay before they reach the decay ring. The ions also have to decay relatively quickly once they are stored.
Good candidates are the noble gases ^6He and ^{18}Ne. An advantage is that they will not bind chemically to the target material, and can therefore be extracted easily.
The shortfall in production of ^{18}Ne has made it necessary to investigate other candidates like ^8Li and ^8B, see [16].

1.1.2 Project description

In Ref. [1] these two ions are considered as an anti-neutrino source (^8Li) and as a neutrino source (^8B). The neutrinos are produced by the reactions

$$^8_5B \longrightarrow^8_4 Be + e^+ + \nu_e$$
$$^8_3Li \longrightarrow^8_4 Be + e^- + \bar{\nu}_e.$$

These nuclei produce relatively high energy neutrinos. Ref. [1] suggests a ^6Li or ^7Li beam as a circulating beam with repeated passes through a wedge-shaped gas-jet-target of ^2H or ^3He to produce ^8B or ^8Li:

$$^6_3Li +^3_2 He \longrightarrow^8_5 B + n$$
$$^7_3Li +^2_1 H \longrightarrow^8_3 Li + p.$$

In our study we will focus on the circulating ^7Li beam to produce ^8Li by passing through a deuterium target. This beam will be stored in a production ring with a kinetic energy of $25\,MeV$ as suggested in [1].
The production ring will be located directly behind the ion source of ^7Li. Also the circumference of this ion ring should be in the range of only a few meters, this is possible due to the low kinetic energy of the ions at this point of the production process of the beta beam. Due to the fact that the target is supposed to

- produce a radio-active ion beam
- strip the incoming beam
- cool the beam

the lattice design has to be such that these three functions of the target are supported.

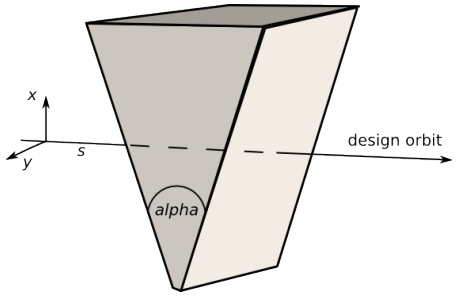

Figure 1.1: Scheme of wedge target

For the particular cooling of the beam in the production ring, a special wedge shape of the target is required, see Fig. 1.1. For further information see [3]. In Ref. [3] a width of the target of $5\,cm$ at the design orbit is chosen. This will not be discussed in detail here, see Fig. 1.1 for the positioning in the coordinate system.

1.2 Introduction to lattice design

In this chapter we will show the most important conventions and parameters in accelerator physics which are essential for the lattice design.

For all calculations we will use the same local coordinate system which is moving along the reference orbit. In a circular machine the elements are placed along the reference orbit which is defined as the trajectory a perfect particle (particle with the design energy of the lattice, $\frac{\Delta p}{p} = 0$, $x = 0$, $x' = 0$, $y = 0$, $y' = 0$) would follow. That defines a right-handed coordinate system (x, y, s), where x is the coordinate in the horizontal plane, the bending plane (positive values to the outside), y is the vertical coordinate (positive values upward) and s is the tangent to the reference orbit.

For the description of single particle trajectories the solution of the Hill's equation

$$\begin{pmatrix} x \\ x' \end{pmatrix} = M \cdot \begin{pmatrix} x_0 \\ x'_0 \end{pmatrix} \tag{1.1}$$

can be used, where x_0 and x'_0 are the coordinates of the starting point and x and x' are the coordinates at the end point of the trajectory which is examined here. The matrix M depends on the properties of the magnets (focusing strength, length, bending radius) which are positioned in between. For every element a individual matrix has to be calculated, to get the transfer matrix for a path passing through several elements these individual matrices has to be connected by matrix multiplication in the order in which they appear in the lattice. These matrices for the different element types (focusing and defocusing quadrupoles, dipoles and drifts) can be found in [5].

This formalism is only valid for a single particle, but in terms of linear beam optics in the case of periodic conditions it is possible to describe the transfer matrix from the beginning of the structure to the end by the so-called Twiss parameters α, β and γ.

$$M(s) = \begin{pmatrix} \cos(\mu) + \alpha_s \sin(\mu) & \beta_s \sin(\mu) \\ -\gamma_s \sin(\mu) & \cos(\mu) - \alpha_s \sin(\mu) \end{pmatrix}$$

The parameters α and γ are related to the β-function by the equations

$$\alpha(s) = -\frac{1}{2}\beta'(s) \qquad \text{and} \qquad \gamma(s) = \frac{1 + \alpha^2(s)}{\beta(s)}. \tag{1.2}$$

Due to the fact that the Twiss parameters depend on s the transfer matrix is also a function of s. The variable μ is called phase advance and is given by

$$\mu = \int_s^{s+L} \frac{dt}{\beta(t)}.$$

The boundary condition for a stable movement of the particles in the lattice is given by

$$\text{stability} \Longleftrightarrow |\text{trace}(M)| < 2 \Longleftrightarrow \mu \text{ real}, \tag{1.3}$$

this marks demands on the focusing properties of the lattice, which also affect the Twiss functions.

The β-function is a periodical function which depends on the focusing strength of the lattice elements. Also the square of the beam size is proportional to the β-function (without momentum spread of the particles or with zero dispersion). The beam size is given by

$$\sigma = \sqrt{\epsilon \cdot \beta},$$

where ϵ is the emittance which is normally given in $[\pi \cdot mm \cdot mrad]$ and is defined as the area of the phase space ellipse divided by π [5]. In case of energy conservation the particles follow, by a given s position, an ellipse in the 2-dimensional phase space x-x' or y-y', because the optics functions recur after one revolution, or in machines with a special symmetry after each period of the symmetry part. If we assume a Gaussian distribution of the particles in the x-x' or y-y' plane, the particle which describes the ellipse at 1σ of this distribution defines the beam size.

Up to now we only consider particles with an ideal momentum p_0. In general the energy or momentum of the particles in a storage ring deviate slightly from the ideal momentum of the beam. This causes an additional factor to the $x(s)$ coordinate which can be described by

$$x_D(s) = D(s) \cdot \frac{\Delta p}{p}.$$

The dispersion function $D(s)$ is defined by the focusing properties of the lattice and the bending strength of the dipole-magnets $\frac{1}{\rho}$. To include this in the calculations of the trajectories, equation 1.1 can be extended to three dimensions; $(x, x', \frac{\Delta p}{p})$.
For further information see Ref. [5] and [6].

2 Lattice Design

2.1 MAD-X

For the design of the lattice the MAD-X (**M**ethodical **A**ccelerator **D**esign) program, a general purpose accelerator and lattice design program, was used. MAD-X is developed at CERN and is the successor of MAD-8 with several additions and extensions, to comply with the LHC requirements.

The program requires two input files, the sequence and the MAD-X-working file.
The sequence file describes the properties of the machine elements (strength, length, multipole order and the position at which they are located in the accelerator).
In the MAD-X-working file the machine description has to be referenced and the beam parameters (name, mass, energy and charge of the particle) have to be set. One of the main objectives is to calculate the optics parameters, the so-called Twiss functions, to obtain the linear beam optics, that corresponds to the chosen lattice elements. With the aid of the TWISS command, it can be chosen between a non-periodic simulation, with given Twiss parameters at the beginning of the sequence (used for open lattices, e.g. for a beam line), or a periodic one (used for closed designs, like a ring accelerator). The periodic solution requires that the values of the Twiss parameters at the beginning of the cell are equal to their values at the end, so that two cells easily can be connected to a section. By varying the strength and the position of the elements the parameters we need (β, α, D_x, D_{px}) can be optimised.
With these commands MAD-X is able to calculate a circular accelerator or a beam line. MAD-X is also able to simulate possible machine imperfections that impacts the beam dynamics.

As an output a file with all Twiss parameters is given and a plot of these parameters through the lattice as a function of the position in the ring can be created. One example of such a plot is shown in Fig. 2.9.

2.2 First steps

Ref. [1] shows an accelerator lattice with four meter circumference, which is compact and symmetric. This chapter will discribe a design based on the proposals in [1]. This circular machine is made of only one basic section with one meter length, repeated four times. The lattice is shown schematically in Fig. 2.1.

The basic cell is made of two quadrupole doublets on each side of the cell dipole. In the straight sections between the cells there are drift spaces, where the target and RF-cavity can be positioned.
In this chapter only the linear lattice design will be explained. The target and cavity implementation or machine imperfections are not included. Some of these will be discussed in the following chapters.

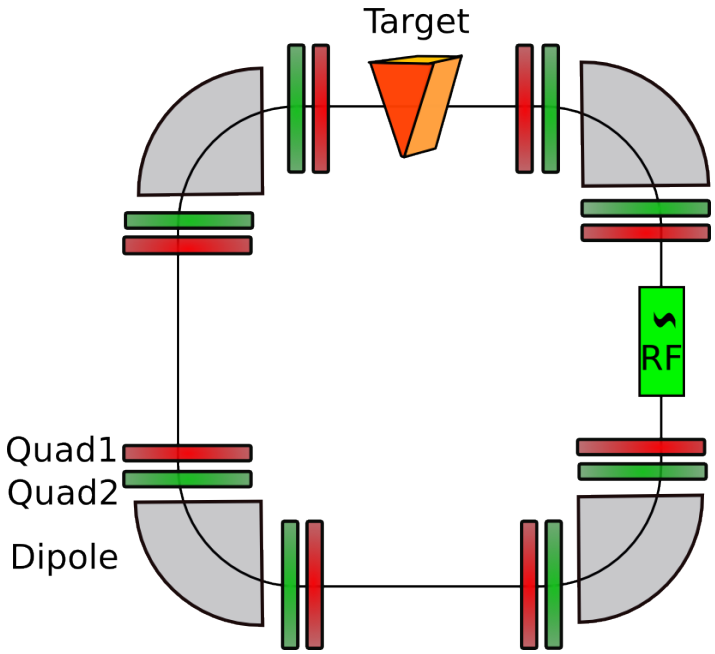

Figure 2.1: First scheme of the ion ring lattice, similar to the design in Ref. [1]

2.2.1 Dipoles

As a first step of the lattice design the geometry of the machine has to be defined. The needed strength of the dipoles is calculated in order to get their length. In a magnetic field the particles get deviated by the Lorentz force F_L:

$$F_L = F_{Centri} \Rightarrow q \cdot v \cdot B = \frac{m \cdot v^2}{\rho} \Rightarrow B \cdot \rho = \frac{m \cdot v}{q} = \frac{p}{q}, \tag{2.1}$$

where F_{Centri} is the Centripetal force. With this relation we are able to determine the beam rigidity $B\rho$ and thus the required dipole field for a given momentum p and charge q of the particles. Since we want to store a fully stripped $25\,MeV$ beam of ^7Li, we get a value of

$$B\rho = 0.64\,\mathrm{Tm}. \tag{2.2}$$

Assuming normal conducting magnet technology for the production ring design the field strength of the dipoles is limited to $B = 1.5\,T$. Equation 2.2 leads us to a bending radius $\rho \geqslant 0.42\,m$. Using only four dipole magnets in the machine design requires a bending angle of $\frac{\pi}{2}$ per dipole and we therefore obtain a minimum arc-length $l_{dipole} = \frac{\pi}{2} \cdot \rho = 0.67\,m$ of the sector-magnets.

2.2.2 Challenges

If we assume the layout which is shown in Fig. 2.1, it has to be pointed out in this context that the overall sum of the dipole lengths is $\sum l_{dipole} \approx 2.7\,m$. Holding, as a first estimation for the length of each of the 16 quadrupoles, a value of $0.1\,m$, see detailed calculation below. The outcome of this rough estimate is that the basic lattice elements require a length of $4.3\,m$. In addition we assume $50\,cm$ drift space between the basic cells and as a realistic estimation $10\,cm$ between the quadrupoles and dipoles, we get a value for the machine circumference of at least $l_{circum} \approx 8\,m$. With thick lenses without using special accelerator techniques, like for instance edge focusing of the dipoles the ring circumference becomes larger than the value in [1].

A small circumference, gives a strong contribution from the dipole magnets to the horizontal focusing of the machine. Because of the small bending radius $\rho = 0.42\,m$ the focal strength,

$$k_{dipole} = \frac{1}{\rho^2} = 5.67\frac{1}{m^2},$$

is large in comparison to the focal strength of the quadrupoles. We will see later that quadrupoles will have values around 20-30 $\frac{1}{m^2}$. Since the $\frac{1}{\rho^2}$ dominates the focusing it is not easy to find a stable solution for such a small lattice. To solve this problem the bending radius, or rather the dipole length, has to be increased, leading necessarily to an increased machine size.

However, a lattice similar to Fig. 2.1 having a circumference of $8\,m$ gave a periodical solution.
This design has to be enhanced to give the possibility to match the values of the dispersion in the area of the target and the cavity, according to the requirements. There are too few degrees of freedom for a good dispersion matching. Only the four quadrupoles per section and the distances between the elements are possible to vary. For the requirements (see next chapter) a matching of at least D_x, $D_{px} \equiv \frac{dD_x}{ds}$, $\alpha_x \propto \frac{d\beta_x}{ds}$ and $\alpha_y \propto \frac{d\beta_y}{ds}$ is needed, and therefore all quadrupoles are required. So this minimal design is a rigid layout, there are no possibilities to match the β-values or the tune.

2.3 Cavity and target requirements

In the region of the cavity the dispersion function D_x has to vanish, not to influence the stability of the beam. The cavity could excite a transversal disturbance, which would decrease the beam lifetime.

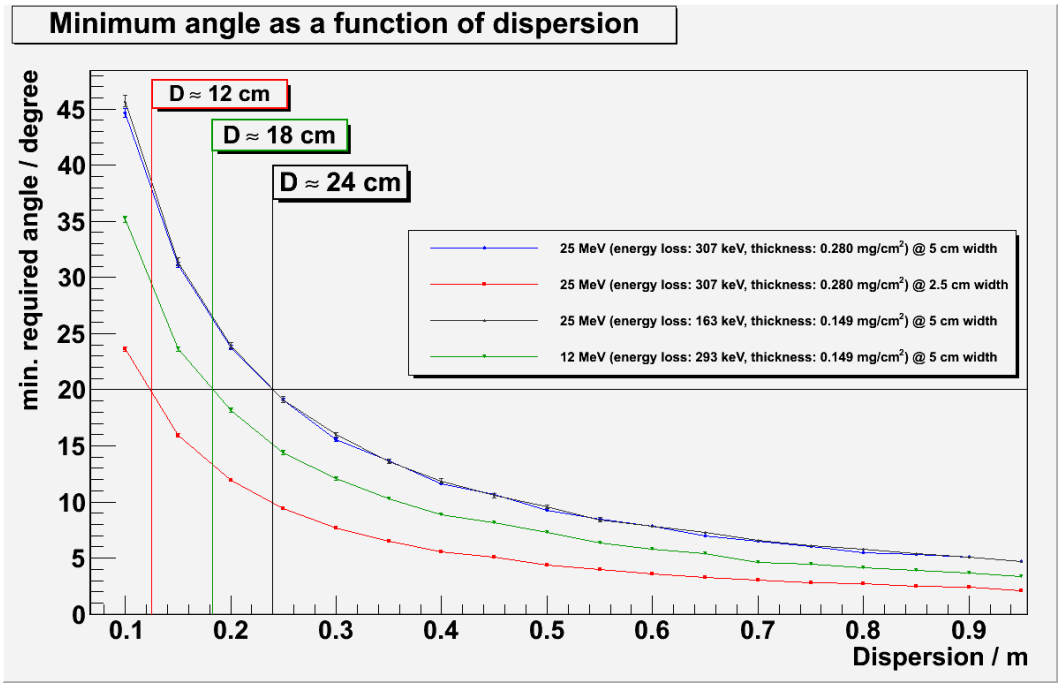

Figure 2.2: Target requirements to the dispersion as a function of the wedge angle, see [3]

The target also requires special dispersion values depending on the aperture angle of the wedge, as shown in Fig. 2.2 [3]. These constrains results from the longitudinale cooling condition which is presented in [1]. This plot displays the necessary minimum angle of the wedge as a function of the dispersion. A $25\,MeV$ beam of ^7Li which passes through a target of a thickness of $0.280\,\frac{mg}{cm^2}$ at a width of $5\,cm$ is shown as the blue curve in Fig. 2.2. If we assume a wedge angle of 20° it can be seen that a minimum dispersion of $24\,cm$ is required. To ensure that there is enough margin in the design of the target a value of $D_x = 50\,cm$ at the target location has been chosen in the lattice design. This gives the possibility to decrease the wedge angle to 10° without considering a change in the dispersion requirements. An increase of this angle is still no problem and can always be done without thinking about a too low dispersion.

For further information of the target design and implementation in Geant4 see [3]. An implementation of a target model in Fortran for use in SixTrack is described below.

2.4 Alternative design

Because of the special requirements of the dispersion, the dipole focusing problems and the limited flexibility of the lattice, we considered additional possibilities for the storage ring layout. As a start we try to find a design with sections where the dispersion is zero, to take the dispersion requirements of the cavity into account. There are two different lattice types which satisfy this and still lead to a compact machine: The double bend achromat and the triple bend achromat.

2.4.1 Double Bend Achromat

The double bend achromat layout is shown in Fig. 2.3 is composed of a symmetric arrangement of two bending magnets around a focusing quadrupole in the centre. The strength of this quadrupole is adjusted in a way that the dispersion generated by the first dipole is cancelled by the second one. All areas outside the block of the dipole segments, are dispersion-free. Also two quadrupole doublets are located on each side of this block of dipole segments. Moreover this layout generally provides a very small dispersion of the bending magnets.

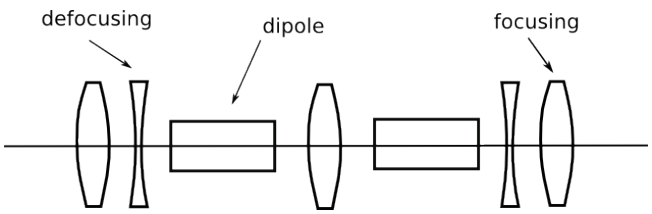

Figure 2.3: Lattice design of a double bend achromat

In this form the structure is still rather inflexible. The centred quadrupole only focuses in one plane, here the horizontal one, and the focusing properties in the vertical plane need special care. It is here corrected by the external quadrupoles at the left and right sides of the dipoles. Another possibility which provides more flexibility, is to locate additional quadrupoles in the space between the bending magnets. Moreover, it is allowed to place more quadrupoles at the ends to increase the flexibility, but this will also increase the circumference of the ring. This scheme is in literature also known as the "(expanded) Chasman-Green lattice" [9].

2.4.2 Triple Bend Achromat

The triple bend achromat lattice (Fig. 2.4) is the logical extension of the double bend achromat structure. An additional bending magnet in the centre of the double bend achromat lattice with a second focusing quadrupole, to obtain the symmetry, is located. This allows extra flexibility.

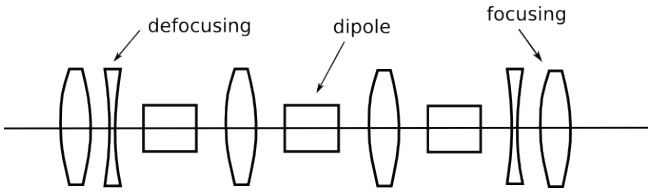

Figure 2.4: Lattice design of a triple bend achromat

In a future optimisation of the lattice which is designed here, one probably has to look at the chromaticity. For chromaticity correction sextupoles are needed and the only area in which they are useful for this aim is between the dipoles, where the dispersion is not zero. In a triple bend achromat the positioning of correction sextupoles is easier and lower sextupole strength is needed, due to the fact that the dispersion is greater than in a double bend structure. Also because there are larger regions with non zero dispersion, the chromaticity can be corrected with a higher accuracy.

2.4.3 First choice

To obtain a compact machine layout and a small number of elements in the ring, the first proposal of the double bend achromat is chosen here. There are only five different quadrupole types in the lattice, three focusing and two defocusing. Maximum symmetry and a small lattice, thus a mirror symmetry is chosen in the middle of each section. A mirror symmetry in the middle of each section gives a small lattice with maximum symmetry. In this way only three different quadrupole families are necessary.

In the following the development process will be described in detail. As a starting condition we aim for a circumference of $12\,m$. However, we start with $18\,m$, because it is easier to begin with a larger machine and then reduce the circumference. At first, the structure of one section is implemented in MAD-X. Four of those will then be connected in series to define the complete ring. The values of the dipole parameters as discussed before ($l_{dipole} = 0.7\,m,\ B = 1.5\,T,\ \varphi_{bending} = \frac{\pi}{2}$) and a quadrupole length of $0.1\,m$ are used for this. It should be noted that the dipole in each section will be cut into two pieces for this design. Each piece has now a length of $35\,cm$ and a bending angle of $\frac{\pi}{4}$. Because we do not know the right values of the quadrupole strengths, some are guessed. We start with a non-periodic calculation. For this we have to choose some Twiss parameters at the beginning of the section as initial values. For the first approximation we do not need to be accurate, but the quadrupole strengths should be in the range of the expected or desired ones. In most cases, the solution will not be stable and the β-function will be very large at the end of the section. In that case the quadrupole strengths have to be varied by hand. It takes some time to get a feeling for that and to get usable results. As a rule of thumb, the necessary condition for a stable motion

$$|\mathrm{trace}(M)| < 2 \Longleftrightarrow \mu\ real \tag{2.3}$$

from equation 1.3 can be used. In the TWISS output MAD-X calculates $\cos(\mu)$ in the vertical and horizontal plane, which have to be smaller than one, because μ have to be real for a stable motion. With this condition the strengths are approximated so that MAD-X is able to calculate a periodic and stable lattice. By looking at the plot of the non-periodic solution, the strengths are changed so that the functions at the end get similar values compared to the starting-point. Now a periodic TWISS run can be started. To get a better and more stable solution, the distances between the elements are at this moment included as free parameters to obtain additional flexibility. In Fig. 2.5 the β-function in the horizontal (red) and vertical plane (green) and the dispersion (blue), calculated by MAD-X are displayed.

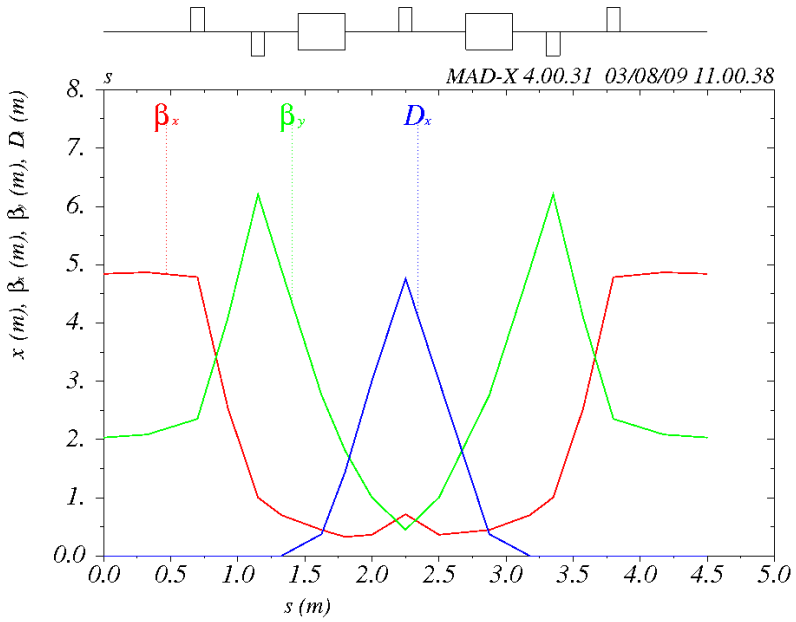

Figure 2.5: One section of a ring with 18 m circumference

It can be seen that the dispersion has a maximum in the middle between the dipoles and is zero in the straight sections. This is exactly what is required.
For this result the dispersion D_x and the derivative of the dispersion $D_{px} = \frac{dD_x}{ds}$ are matched to zero at the beginning and at the end of this first section. Because these are symmetry points of the lattice, also α_x and α_y, which are proportional to the derivative of the β-functions, are matched to zero. As a second advantage, this design is very stable and flexible, which means that the distances and constraints can easily be matched. It is really important that the quadrupole in the middle has the right strength and a large enough distance from the dipoles, otherwise the quadrupole is not able to constrain the dispersion in this way.

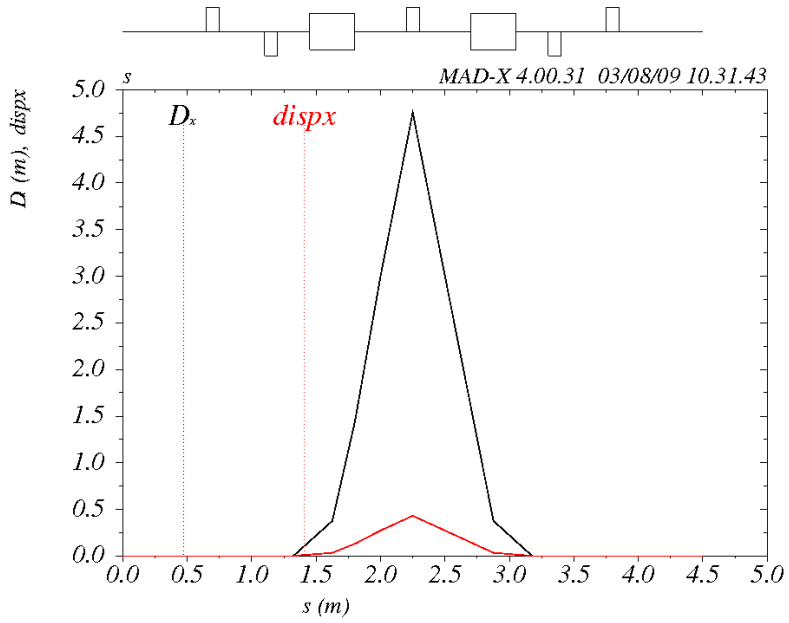

Figure 2.6: Comparison of the dispersion D_x, calculated by MAD-X, and the real dispersion *dispx*

Fig. 2.6 shows a very important detail of MAD-X. The dispersion which is calculated by MAD-X is not the real one, it's value is normalised to the relativistic β-factor:

$$D_{real} = D_{MAD} \cdot \beta_{rel}.$$

In large accelerators with high energies this is not a problem and can be neglected, because there the velocity is near the speed of light and β_{rel} is near one. In our case, a kinetic energy of only $25\,MeV$ is used, and $\beta_{rel} \approx 0.09$. So the real dispersion is around $10\,\%$ of what is calculated by MAD-X. This results from a coordinate transformation which is used in MAD-X internally.
This has to be remembered when other parameters calculated by MAD-X are considered, e.g. the chromaticity.

Four of these sections are linked together to obtain the complete ring. The ring circumference is then reduced, step by step, to the wanted $12\,m$. A step size of $2\,m$ is chosen, which works well. In each step the distances between the elements are reduced and after that a new matching, as explained above, is performed.
After getting a solution for the $12\,m$ circumference, as shown in Fig. 2.5 for the $18\,m$, we concentrate on the target location.

At the moment the lattice is perfectly symmetric and consists of four equal parts. Only three quadrupole families are included. Each section is mirror symmetrical with respect to the centre of the quadrupole in the middle between the two dipole segments. As noted before, a dispersion of $50\,cm$ is required in the region where the target is located. Because of this, there are two possibilities to position the target.
The first one is in a straight section. Then the dispersion has to be matched from zero to the desired value at the position of the target, which may be difficult to achieve.
The second idea is to put the target between the two dipole segments. Here the dispersion has a value unequal to zero, consequently it may be easier to match it to $50\,cm$. However, in this region the dispersion is not constant through the target and will vary. This could be a problem for exact simulations. In addition the mirror symmetry would be lost, since the target cannot be positioned in the middle between the dipoles, because the space is occupied of the located quadrupole.
In fact both possibilities can be considered in principle and may lead to an acceptable layout. In this thesis the main focus is concentrated on the first option which is examined in detail below.

We have to give up the four fold symmetry. Now there will be a two fold symmetry, so that the whole ring consists of two equal sections, each with four dipoles of $0.35\,m$ length and ten quadrupole lenses, see Fig 2.8. Again this concept leads to a high symmetry, which gives a good stability and makes it easier to match.
The cavity has to be located in a region with zero dispersion. This implies that the matching for the half ring section has to be more specific than the last ones. Let's assume that this half ring section begins with a possible cavity position. The lattice then begins with a zero dispersion area. Here D_x and D_{px} have to be zero. In the middle of this section the target is positioned. Here the dispersion should be larger than $50\,cm$, so the matching constraints are set to $D_x > 5.8\,m$ (MAD-X convention) and $D_{px} = 0.0$. It is not wanted to give a too strict condition at this point, because it isn't necessary here, $50\,cm$ is only a minimum limit.
At the end of this part of the ring, the same conditions as at the beginning should be satisfied. Also α_x and α_y have to be zero at these three points, i.e. the β-functions should be constant, $\beta' \equiv 0$.

With some effort we come to the results shown in Fig. 2.9. In this plot the horizontal (red) and vertical (green) β-functions and the dispersion (blue) are shown as a function of the local position in the ring. On the top of the plot the position of lattice elements are displayed. We can see that the slopes of the functions are zero at the special symmetry points at $s = 0$, 3, 6, 9 and $12\,m$ which were mentioned above. The boundary conditions $\alpha_x = 0$, $\alpha_y = 0$, $D_{px} = \frac{dD_x}{ds} = 0$ at these points are fulfilled. This contains the mirror symmetry in the middle of the lattice at the chosen cavity position at $s = 6\,m$. In addition the dispersion is zero at this location and has a value of $50\,cm$ where the target will be placed (at $3\,m$).

Furthermore, since the beam size $\sigma = \sqrt{\epsilon\beta}$ is proportional to the square root of the β-function in the accordant plane, we can see that the beam size is varying as the beam passes the different elements and that its transverse cross-section has an elliptic shape which changes all through the machine. We also see from figure 2.9 that in the area of the bending magnets the transverse cross-section is more circular (the β-functions have nearly the same size). In table 2.1 and Fig. 2.7 the most important lattice parameters can be found.

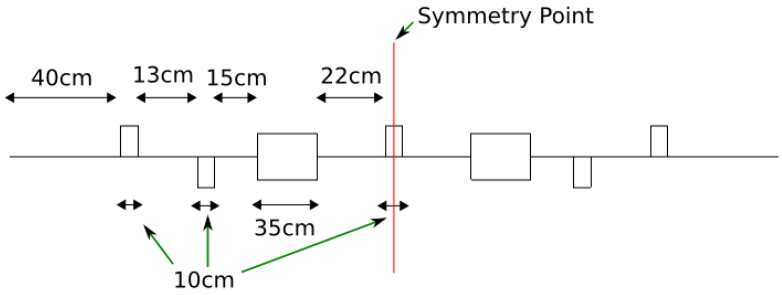

Figure 2.7: Distances and lengths of the elements, one quarter of the ring is shown.

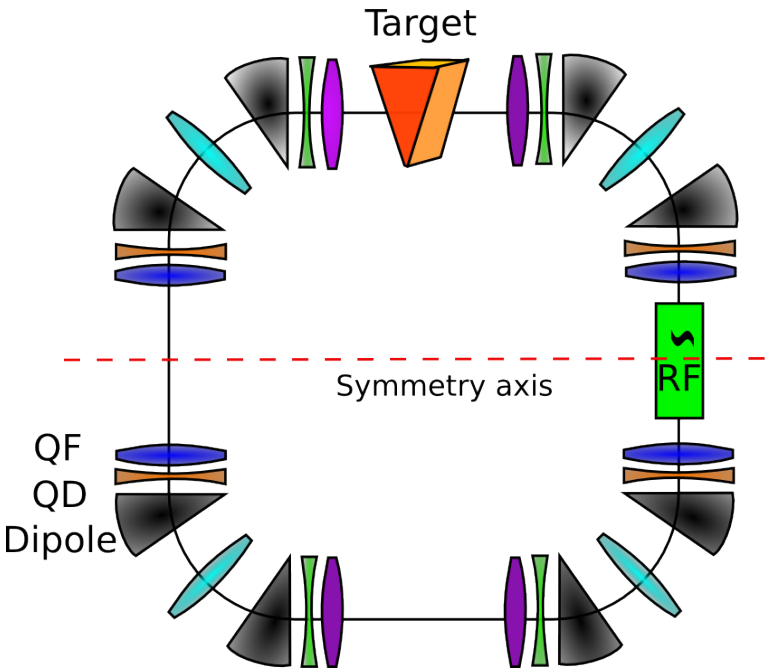

Figure 2.8: Scheme of the final lattice design, (same colour = same strength)

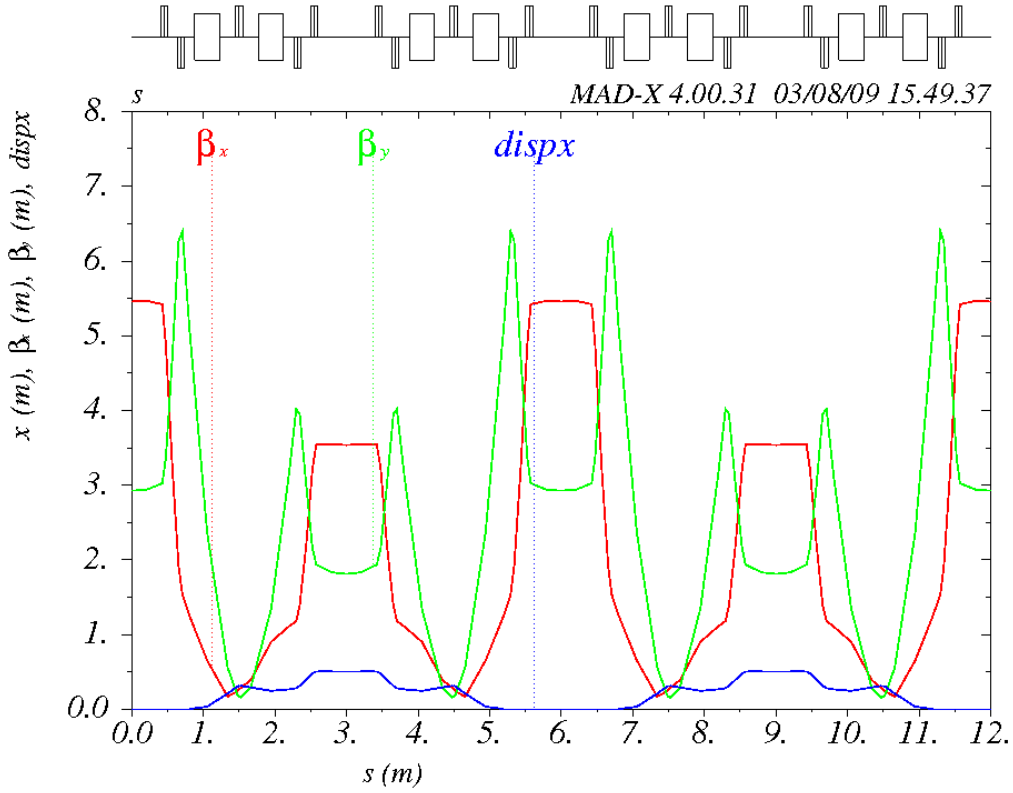

Figure 2.9: First lattice design of the 12 m ring

Lattice parameters

horizontal tune	Q_x	2.47
vertical tune	Q_y	1.86
Gamma transition	γ_t	3.59
Quadrupole strength $[\frac{1}{m^2}]$		
focusing 1	qf_1	21.15
defocusing 1	qd_1	-27.15
centre focusing	qf_m	29.67
defocusing 2	qd_2	-27.94
focusing 2	qf_2	19.79

Table 2.1: Lattice parameter of the lattice shown in Fig. 2.8 and 2.9

2.5 Optimisation

2.5.1 Tune

The results in Fig. 2.9 are obtained with only four constraints in every quarter of the ring. Thus one degree of freedom is left, which means that it is possible to match explicitly one more lattice parameter to a desired value. After careful investigation of the beam parameters listed in table 2.1, it can be seen that the horizontal tune is close to the second order resonance $2.5 = \frac{5}{2}$.
Certain fractional values of the tunes have to be avoided as they lead to resonant excitation and possible loss of the beam. If the condition

$$nQ_h + mQ_v = l \tag{2.4}$$

is fulfilled, with n, m and l integers, the tune catches a resonance of order $|n| + |m|$. Moreover, errors in the magnetic fields cause a finite width of the working point (fractional parts of the tunes) and of each resonance-line. This makes it more difficult to find a good place for the working point.
For an acceptable beam life time, resonances at least up to the fifth order have to be avoided [8]. Fig. 2.10 shows a so-called working diagram up to this order. In such a diagram the fractional parts of the horizontal and vertical tunes are plotted against each other. Moreover the resonance lines from equation 2.4 are displayed in this plot up to an optional order, thereby it is easy to see if the tune hits a resonance.
The yellow dot marks the working point of our production ring. It can be seen that the point is surrounded by several of resonance-lines. Therefore it is possible that the working point covers resonances of the sixth order or higher which are not printed in the plot.

The yellow line marks the coupling resonance which is given by the condition

$$Q_x = Q_y. \tag{2.5}$$

Around this resonance there is more space to put in the working point without covering other resonances, so the tune should be located near that line. It is clear that in general one is interested to place the working point in an area without resonances. It is also important to find a region where the working point can easily be shifted. Once the accelerator is built the magnets have field errors of higher multipole orders. These errors have to be measured and can be taken into account once these measurements are available. Experience exists from earlier magnet production and can be used statistically for new machine design. Consequently errors may change the tune, therefore some freedom must be left to shift the Q-values without hitting resonances. This can be done by varying the magnet strengths carefully, preferably using corrector magnets specially designed for this purpose.

Now we will try to optimise the tune. Normally we have only one degree of freedom

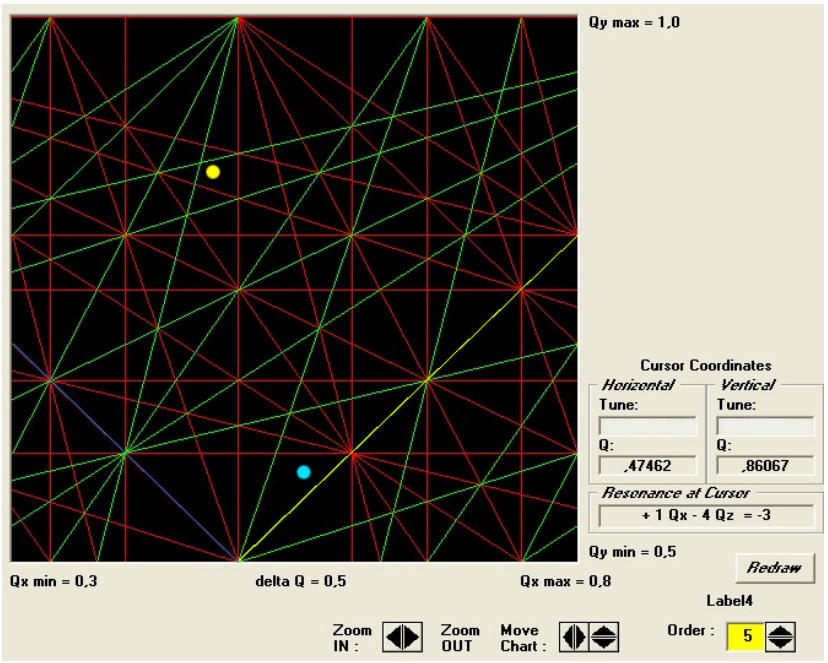

Figure 2.10: Working diagram up to the fifth order

left, but we know that our lattice is symmetric, more exactly it is mirror symmetric. From that two constrains of the matching can be left out. The symmetry requires that α_x and α_y are zero at the symmetry points we choose as matching constrains. After a check with MAD-X, in principle two more degrees of freedom per quarter are free. So it is possible to match the tune in both planes and there is still one degree of freedom left to vary and to optimise for example the β-function.

Also thanks to the symmetry it is possible to vary the tune in a wide range and the Q-values can easily be chosen between the best options. At this stage of the development process it is not clear which is the best approach. An example of an other working-point, located closer to the coupling resonance will be shown to demonstrate the options the lattice layout offers for further optimisation.
The new tunes are found by a global matching and listed in table 2.2 with other significantly changed lattice parameters. The new working point is shown in Fig. 2.10 as the blue dot.
These tunes are chosen to get smaller maximum β-functions and therefore a smaller beam size.

It is important to build the lattice as flexible as possible to be able to adjust the tune independently in the tune diagram until the optimal point is found. The optimal working point is usually found after the preliminary design of the machine lattice.

Lattice parameters after optimisation

horizontal tune	Q_x	2.56
vertical tune	Q_y	1.59
max hor. β [m]	$\beta_{x_{max}}$	5.10
max vert. β [m]	$\beta_{y_{max}}$	4.84

Table 2.2:

2.5.2 Quadrupole length

In this chapter we will have a closer look at the length of the quadrupoles which was up to now only a rough estimation. For the strengths in table 2.1 a length of $10\,cm$ was assumed. Is it possible to build the quadrupoles, in an reasonable way, shorter to reduce the circumference of the ring? Or do we have to provide superconducting technology to build theses strengths by this length?
In the following again a rough estimation will be performed. For a calculation of the strength a beam pipe radius r_0 and for that the beam size, given by

$$\sigma = \sqrt{\epsilon \cdot \beta} \tag{2.6}$$

as a first approximation without momentum spread of the particles, are needed. Where ϵ is the emittance and β is the β-function in one plane. To get reasonable values for the beam size the maximum β-function of the lattice in the vertical plane of circa $6.5\,m$ is used, this produces the largest beam size. Also the equilibrium emittance given in [1] to $\epsilon = 6.6 \cdot 10^{-6} \beta\, m\, rad$ is used. But here one has to notice that this value is calculated only for the simplest case of a ring with a target foil and a cavity. Only multiple scattering is considered. Therefore this can only be treated as a lower limit for the emittance. In the real ring the investigation of this will be more complex. Furthermore the emittance in the ring depends on the emittance which is provided by the ion source and up to now there is no specification of the source emittance. For the moment we will choose the emittance from [1] to make an estimation.
With formula 2.6 the beam size is calculated to $\sigma = 17\,mm$, from the assumption that the beam has a Gaussian distribution this is only a 1-σ interval of the real beam size. To avoid to many particle losses, the inner radius of the pipe is set to 6σ. For accelerators with longer beam life time 10σ would be chosen [6], but since in this case only around 10,000 turns are required, it is allowed to reduce this to 6σ to keep the beam pipe smaller. Moreover, the pipe thickness has to be taken into account. Assuming a thickness of $3\,mm$, including also some tolerance, as an average value, altogether a aperture radius of $r_0 = 105\,mm$ is needed which is large but for an ion ring a reasonable value.

From the necessary quadrupole strengths of around 20-30 $\frac{1}{m^2}$ the magnetic field gradient g and hence the pole-tip-field B_{max} can be computed, form these relations;

$$\begin{aligned} k = &\quad \tfrac{q}{p} \cdot g \\ B_{max} = &\quad g \cdot r_0, \end{aligned}$$

with $B\rho = \frac{p}{q} = 0.64\,Tm$ as calculated in equation 2.2. From this it follows that

$$\begin{aligned} g_{min} = &\qquad 0.64\,Tm \cdot 20\,\tfrac{1}{m^2} = 12.8\,\tfrac{T}{m} \\ g_{max} = &\qquad 0.64\,Tm \cdot 30\,\tfrac{1}{m^2} = 19.2\,\tfrac{T}{m} \end{aligned}$$

$$\begin{aligned} \Rightarrow B_{min} = &\quad g_{min} \cdot r_0 = 12.8\,\tfrac{T}{m} \cdot 0.105\,m = 1.34\,T \\ \Rightarrow B_{max} = &\quad g_{max} \cdot r_0 = 19.2\,\tfrac{T}{m} \cdot 0.105\,m = 2.02\,T. \end{aligned}$$

Such a small ring is typically built with normal conducting magnets, therefore the magnetic field strength of the quadrupoles is limited up to $B = 2\,T$. One see that the field strength is not necessarily in the superconduction scope, but due to the used minimum value of the emittance, the beam size will be greater in general, and therefore the pole-tip-field will greater too. To lower the pole-tip-field one has to increase the quadrupole length. Since the focal length of a quadrupole is given by

$$f = \frac{1}{k \cdot l},$$

a linear relation between the focusing strength and the length is obtained. So it is straightforward to decrease the field strength by increasing the length.
As an example for a realistic estimation the equivalent length with a pole-tip-field of $B = 1.5\,T$ is now determined to

$$l_{max} = \quad 14\,cm.$$

We have to reconsider the quadrupole length, when a more reasonable value of the emittance is available. Then it will be necessary to recompute a novel lattice with the corrected lengths. The k-values calculated by MAD-X are only theoretical values and it is necessary to control, if the magnets are possible to build in a real accelerator.

2.5.3 Further improvements

The version of the lattice which is described in this thesis is not fully optimised. Only the very basic things are considered. A truly flexible and compact layout with a low number of elements has been created. It fulfills the boundary conditions given by the special target and it fulfills the cavity requirements.

A novel matching of the strengths and the distances between the elements has to be done with the expanded quadrupole lengths when a reasonable value of the emittance

is available. Furthermore the tune has to be checked. This can be adjusted with a tracking program, which will show whether a higher resonance will be hit and lead the particles to a similar trajectory after some turns.

Also the very high chromaticity has to be considered. This should probably be corrected by sextupoles. The sextupoles have to be integrated in the machine in a area with non-zero dispersion, for example in the spaces between the dipole magnets or in the target area.

The particles are supposed to loose approximatly 300 keV of their energy in the target and then passes through the quarter of the ring between the target location and the cavity, where they get this lost energy back. It may have crossed your mind, that in that quarter the energy of the beam is around one procent smaller than in the rest of it. One has to take into account that under these conditions the particles see the forces of the magnets which are computed for their intended energy, thus they get distracted in the wrong way. This circumstance could cause more particle losses. Calculations should be made to investigate if this is of importance or if it can be neglected. Maybe the magnet strengths have to be adapted to the energy in this section separately.

Other options are still open for the lattice layout, such as the use of rectangular dipoles with edge focusing instead of sector magnets, in order to decrease the ring circumference, by decreasing the focusing strength of the dipoles.
Also it will probably be necessary to add some coupling elements (skew quadrupoles or a solenoid), for cooling considerations [2].
Another option which has been mentioned above, is to put the target between the dipole segments. In this area there is still dispersion which is essential for the location of the target. For that idea the solution from Fig. 2.5 has to be modified. Here the dispersion has a triangular behaviour and this could be a problem for the functionality of the target, so it has to be flattened. This can be done by increasing the distances between the dipole segments and the centred focusing quadrupole, which would be necessary anyway. Because for the target itself and the ring device, which will extract the produced ^8Li ions behind the target, space is needed. It can be also supported by additional quadrupoles in between, like shown in paragraph 2.4.1 and 2.4.2 about the double and triple bend achromats. It may turn out that this is a more reasonable position for the target concerning the dispersion and that it is possible to decrease the circumference of the production ring considerably.

3 The production target

In this chapter we will have a closer look on the target. As already explained in chapter 1.1.2, our accelerator will have an internal target to produce the radioactive isotopes. The particles which will pass through it and which will not undergo any nuclear reacion, will get scattered and will loose energy. In principle the RF cavities will restore the longitudinal energy component, thus providing a net cooling of the beam.
The production target has been extensively studied in [3]. We will here discuss the way to include it in the tracking simulations. Surely the existing implementation of the target in Geant4, developed by Jakob Wehner [3], could be linked to available tracking code. But calling an external program for each turn when the particles hit the target to simulate the target properties would increase the runtime exponentially and would be difficult to realise. It has therefore been decided to implement an analytical model for the target, in order to speed up the tracking simulations.

The idea that will be presented here, is based on the comparison of established formulas to the simulation which is done with Geant4 in [3]. The use of these formulas will simplify the implementation, but only be an analytic approximation of the particle behaviour in the target.
As a first estimation we will only study how the target influences the beam and how the emittance is influenced.

The main purpose of such a target is to produce ions of ^8Li in a high rate, but not all ^7Li particles which hit the target are producing ^8Li, most of them are only scattered. This means that the routine has to estimate the scattering angle. Out of that, the new directions of the particles after the target can be calculated. Moreover, the target produces an energy loss of each particle passing through the target. For the moment we only implement these two reactions of the beam with the target. Lets assume that these effects are independent.

3.1 Energy loss

Every particle loses energy when it passes through matter, this effect is described by the Bethe-Bloch formula for relativistic and non-relativistic particles. From this we compare the resultes from the simulations using the Bethe-Bloch formula with the simulated data from Geant4, as shown in Fig. 3.1 [3].
To simplify the implementation the Bethe-Bloch formula is not integrated over the range of the target matter in this case; we assume constant thickness of the target

for all particles. Due to the wedge shape of the target the thickness depends on the x-offset of the individual particle. The low kinetic energy of the particles ($25\,MeV$) allows to neglect the relativistic correction. As we can see, for lower energies the Bethe-Bloch formula does not give the same results as the simulated data, but with increasing kinetic energy the results are well in agreement. Assuming the storage of a $25\,MeV$ beam of ^7Li, the approximation of the energy loss with the Bethe-Bloch formula seems to be a good approach. If in the future we will find that a lower energy of the beam would be better, this model is not appropriate.

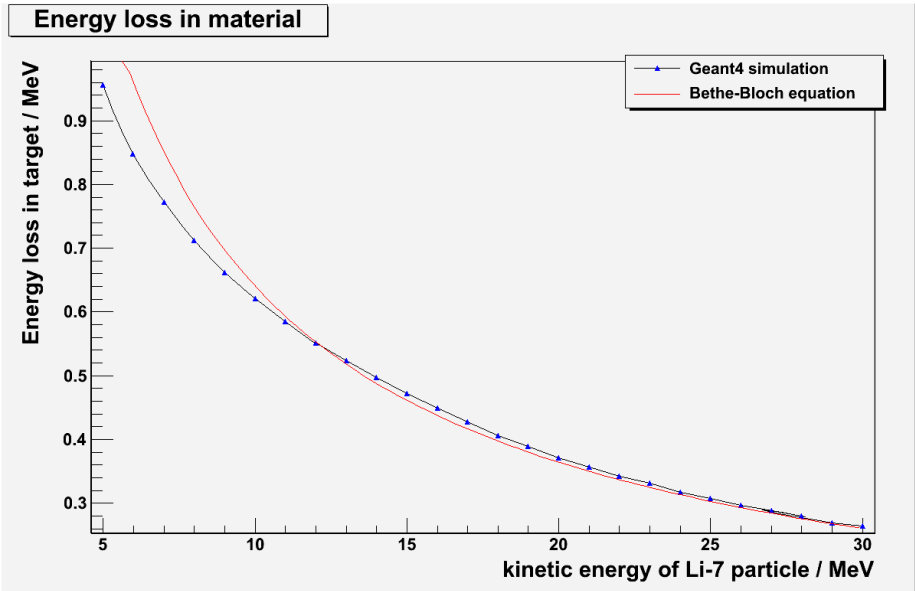

Figure 3.1: Comparison of the Bethe-Bloch formula (red) to the simulated data from Geant4 [3]

3.2 Multiple Coulomb scattering

The second effect on which we will focus here is to describe the scattering of the incoming ^7Li ions on the deuterium gas in the target. A charged particle passing through matter is deflected by many small-angle scatters. Most of this effect is due to the multiple Coulomb scattering, which is roughly Gaussian for small deflection angles. Reference [10] describes this and suggests that it is sufficient to use a Gaussian approximation for the central 98 % of the projected angular distribution, with a width given by

$$\theta_0 = \frac{13.6\,\mathrm{MeV}}{\beta cp} z \sqrt{\frac{x}{X_0}} \cdot \left[1 + 0.038 \cdot ln\left(\frac{x}{X_0}\right)\right]. \tag{3.1}$$

Where βc is the velocity, p the momentum, z the charge number of the particle and $\frac{x}{X_0}$

is the thickness of the scattering medium in radiation lengths. The radiation length

$$X_0 = \frac{716.4\,\frac{g}{cm^2} \cdot A}{Z(Z+1) \cdot ln(\frac{287}{\sqrt{Z}})} \tag{3.2}$$

is a characteristic of a material, related to the energy loss of high energy, electromagnetically interacting particles. Here Z is the atomic number and A is the mass number.

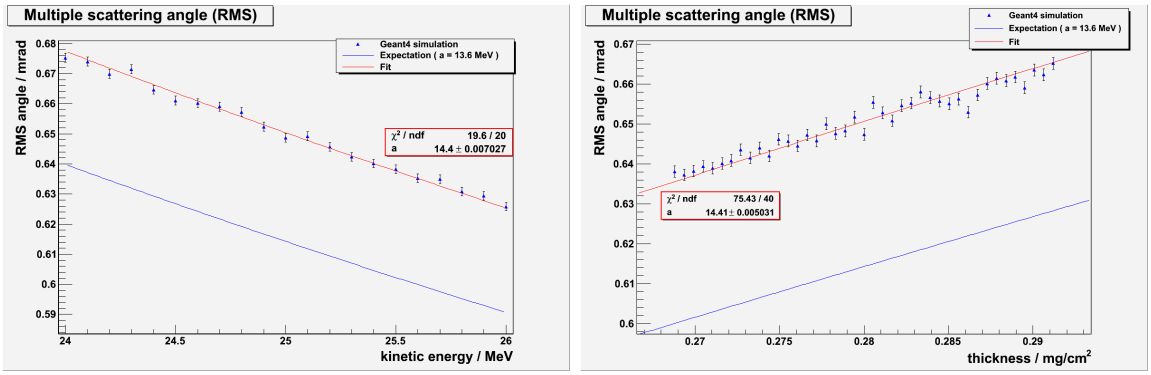

Figure 3.2: Comparison of equation 3.1 to the simulated data of Geant4 [3]

With the aid of equation 3.1 we are able to calculate the RMS of the scattering angle distribution as a function of the kinetic energy and the thickness of the target. A comparison to the Geant4 data simulation is displayed in Fig. 3.2. At the left side you can see the RMS (blue) as a function of the kinetic energy of the incoming particles at a constant thickness of $0.280\,\frac{mg}{cm^2}$ at a width of $5\,cm$, on the right as a function of the thickness at a constant kinetic energy of $25\,MeV$. As it is convenient to see there is an offset between the expectation and the blue Geant4 data dots. In fact it seems to be a similar behaviour except for the offset in the RMS scattering angle.
We assume that the Geant4 simulated data is correct, but equation 3.1 is only valid for singly charged particles with a $\beta_{rel} = 1$ for all Z, accurate to 11% or better for $10^{-3} < \frac{x}{X_0} < 100$. In our case a $\beta_{rel} = 0.09$ and a $\frac{x}{X_0} \sim 10^{-6}$ is used. So we are out of validity range of this formula. To act on the assumption that the parameters in equation 3.1 come out of a fit, we try to fit the parameter $a = 13.6\,MeV$ in 3.1 to a value giving similar results as Geant4 [3]. The results are also plotted in Fig. 3.2, red curves. The new fit parameter, coming out of our fit to the Geant4 data, $a_E = 14.4$ and $a_{th} = 14.41$ are compatible with each other in an 1-σ interval. For the estimation of the target, now equation 3.1 with the new fit parameter $a = 14.41$ is used to calculate the RMS of the scattering angle distribution at different kinetic energies. For further information see [3].
It is assumed that a particle only changes its direction and not its position when itpasses through the target, the target will not cause a new x- or y-offset, but it will change the angle.

3.3 Implementation

The target model will be implemented in SixTrack [11], a tracking code extensively used at CERN and chosen for our studies. The target will be included in the code as a subroutine composed of four functions and written in Fortran 77, since this is the programming language of SixTrack.

This target model takes the particle parameters before the target, adds to the incoming values a change in the x' and y' coordinates, caused by the scattering of the ^7Li ions on the ^2H ions of the target, and subtracts the absolute value of the energy loss from the kinetic energy of the incoming particle. After that the novel values are returned to the main program. In fact the thick target is replaced by a kick in the direction, which is a rough approximation.

For the time being, most of the parameters are constants in the routine. The routine simulates a passing ^7Li beam through a target of which the properties are fixed. A thickness of $0.280\,\frac{mg}{cm^2}$ at a width of $5\,cm$ at the design orbit is used, also the wedge angle is set to 20°. If one wants to change them, it is necessary to access the source code.

The first function determines the mean energy loss of the particles with the Bethe-Bloch formula as a function of the kinetic energy and the thickness of the target. Because of the wedge shape of the target, the last one depends on the x-position of the incoming particle.
The second one calculates the RMS of the scattering angle distribution as from equation 3.1 and 3.2 and the new fitted parameter $a = 14.41$, also as a function of the kinetic energy and the thickness.
The last two functions are needed for the random number generation. Given uniform random numbers from a generator of the CERN library are converted into a Gaussian distribution with a mean of 0 and a standard deviation of 1. This normal distribution is then used to calculate a distribution with an optional mean and standard deviation. When this routine is called in the main part of the target routine the mean and the standard deviation have to be given as parameters.

The target routine is a function of x, $x' = \frac{dx}{ds}$, y, $y' = \frac{dy}{ds}$ and the kinetic energy. Also it requires as an argument the number of particles in one array, which is usually 64 (explained later).
With the given constants and the x-position, the real width of the target is calculated for each particle:

$$d(x) = d + 2 \cdot x \cdot tan\left(\frac{\alpha}{2}\right)$$

where α is the wedge angle and $d = 5\,cm$ the reference width at the design orbit of a perfect particle. With that value the individual thickness is determined.

Assuming a normally distributed energy loss, which is maybe not accurate in this energy range, the mean is computed by the Bethe-Bloch-routine. The RMS of this distribution is then, as the average value of Geant4 simulated data for all ions, $\sigma_{Eloss} = 0.027\,MeV$. The Geant4 simulation shows that the RMS values of the energy loss for particles with different $\frac{\Delta p}{p}$ are all very similar, therefore it is reasonable to use the average of these. Also for the change in direction, a Gaussian distribution is assumed, having a mean of 0 and a standard deviation calculated from the second routine.
As a last step these modifications of the particle characteristics have to be taken into account to create the new ones after the target.

3.4 Basic checking of the functionality

It is important to check if the target is working correctly, so at this point a rough checking should be performed. Two things are going to be tested, firstly if the random number generator generates the right distributions in the right range, secondly, we will perform a closer investigation of the energy loss in the target.

3.4.1 Random numbers

The random number generator should produce a Gaussian distribution with an optional mean and standard deviation. For this the target routine is modified: the main part of that routine does not calculate the novel values of the kinetic energy and the direction any longer. It just writes the changes of these parameters into an output file. Ten-thousend particles with the same initial coordinates and energy are sent through the target. Now two histograms are filled with the data from the energy loss and the scattering angle of each passing particle. A Gaussian fit at these histograms is done, Fig. 3.3.

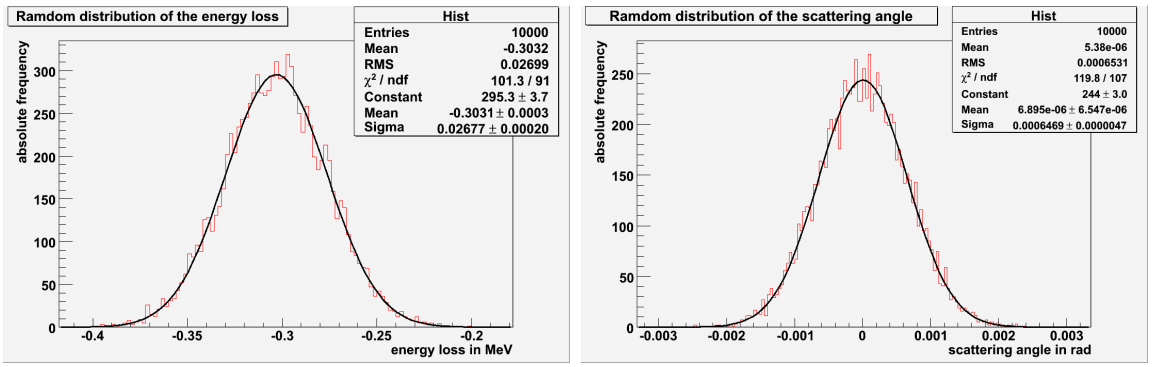

Figure 3.3: Random distributions which are produced by the target routine for the energy loss (left) and for the scattering angle (right)

The figure shows that the Gaussian fits suit well the data, a χ^2 of 1.1 is calculated. The mean of the energy loss per cycle results in $\Delta E = -303.1 \pm 0.3\, keV$, as it is expected. As well, the standard deviation is compatible with the given value. The mean of the scattering angle distribution is around zero, as it is given in the routine. The standard deviation results to $\sigma_{ang} = 0.647 \pm 0.005\, mrad$.

3.4.2 Energy loss

By traversing the target the particles loose in average around $300\, keV$ of their energy and without a cavity, which gives this energy back to them, they would loose their kinetic energy after a few turns. However, this process is not linear, it follows the rules of the Bethe-Bloch formula and the loss gets stronger with lower energy.
A particle has to pass through the whole ring before it comes back to the target and therefore it gets influenced by the lattice elements. In fact it will have different incoming coordinates when it arrives at the target at the next turn. To simulate this without using a tracking code the transfer-matrix through the whole ring (one-turn-map) is computed in three dimensions ($\vec{x} = (x, x', \frac{\Delta p}{p})$) to calculate the new initial coordinates in front of the target after on turn. The new coordinates are then given by

$$\vec{x} = M \cdot \vec{x_0}.$$

Now one particle is sent through the machine for 45 turns, and its coordinates are re-calculated in that way for every cycle. In picture 3.4 the energy trend of such a particle is plotted in red. The energy scale is here around $950\, MeV$ because the routine should be compatible to the future tracking code and SixTrack is only able to track protons or electrons, therefore an equivalent energy for a proton has to be computed, see below.

In comparison to this the black curve represents a particle with equal start parameter before every target hit. It is convenient to see that the black one loses more energy than the red by equal initial parameters. This is easy to understand, because the black particle passes the same width of the target in every turn (here $d = 5\, cm$). On the other hand the red one passes the target in every cycle at a more negative x-position which is caused of the smaller energy, thus the scattering angle and hence the direction of the particle is changed and transferred through the machine. It sees a smaller width of the target and from there it loses lower energy.
The reason for the low number of turns results from the small start energy, the ion has lost nearly its total kinetic energy in this first few turns without the acceleration of a cavity. This is exactly the effect which is expected and shows that the target is working in principle.

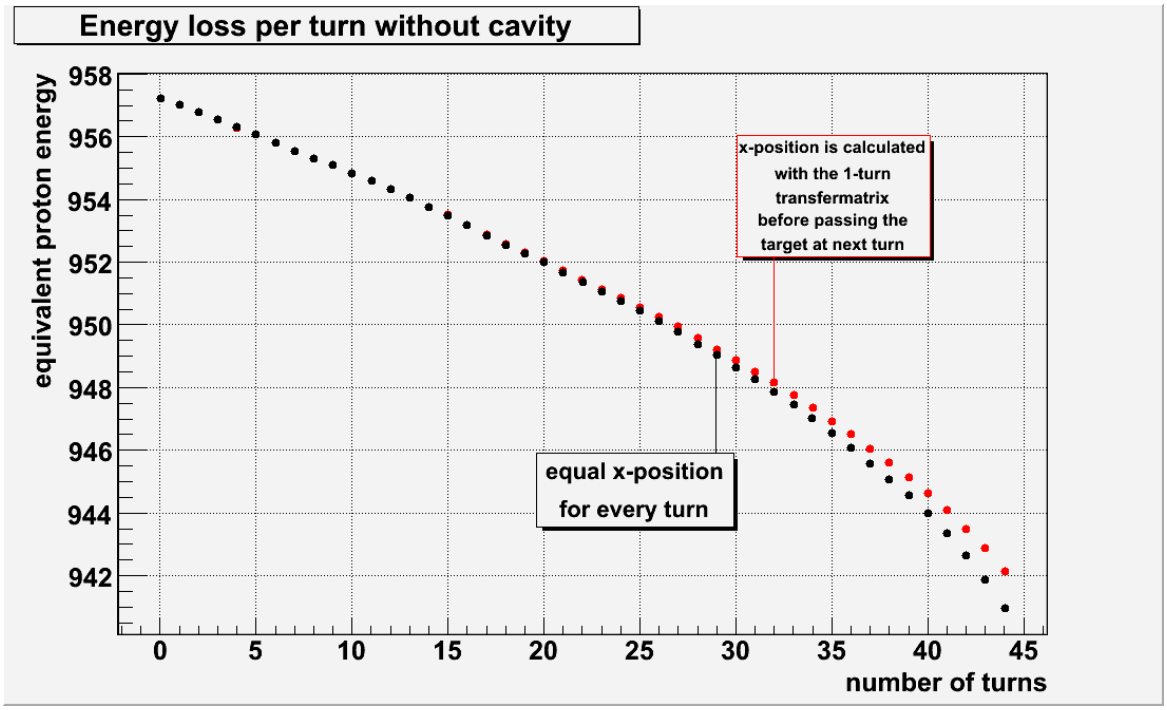

Figure 3.4: Energy trend of two particles with equal initial coordinates, which follows different definitions of evaluation for these parameters. We assume that the RF cavities are off, therefore the energy lost at the target is not restored.

4 Tracking simulations

4.1 SixTrack

For the tracking simulations of the Litium ions in our accelerator and through the target, we chose to use SixTrack [11], a tracking code developed and widely used at CERN. This code is full six-dimensional, single particle and includes synchrotron oscillations in a symplectic manner. Normally this code examine pairs of two nearby particles, to account their behaviour in the phase space and to check if their motion is regular or chaotic.

The original SixTrack code is limited to track a maximum number of 32 pairs of particles, but for the treatment of the production ring many more are required, therefore an existing extended version of SixTrack is used. This version is developed for the LHC collimator studies [12] and permits a tracking of a variable number of particles. This modification is based on an adjustable number of arrays of 64 particles which is compatible to the original code. Moreover, each time, an element in the lattice is recognised as a collimator, special additional routines are called. These features will be used to implement the production target in that code, as if it was a special kind of "collimator".

The main reason to choose SixTrack for the tracking calculations is based on the fact that it is a six-dimensional code, therefore it is possible to include cavities. Other tracking codes like ICOSIM are only four-dimensional and not able to work with cavities, but this is a basic necessity for this production ring, because of the energy loss. Moreover, it is easier to integrate a target into the extended version of SixTrack which is used here, than in other programs.

On the other hand, SixTrack only can treat protons, therefore an equivalent energy for a proton beam has to be calculated.
All dipole and quadrupole strengths in the machine are adapted to a ^7Li beam of $25\,MeV$. This causes out from equation 2.1 a beam rigidity $B\rho = \frac{p}{q}$ of $0.64\,Tm$. Because the built lattice is based on this value, it has to be preserved when the beam energy is converted to an equivalent proton beam, therefore it is easy to evaluate this energy. The beam rigidity includes the charge and the momentum of the particle and this is all what differs the two beams. A proton carries a charge of $q = 1e$, when e is the elementary charge, in comparison to the ^7Li which carries $q = 3e$. The conservation of the beam rigidity results the sought kinetic proton energy of $19.18\,MeV$. Now this novel beam has to be employed in SixTrack.

Input files

For the work with SixTrack several 'fort.*' files are required. The most important ones are the 'fort.2' file and the 'fort.3' file.

The fort.2 file contains the lattice structure. This file can be produced as an export file form MAD-X via the SIXTRACK command.
SixTrack works exclusively with thin lenses, all elements (except drifts) must have a zero length and have to be replaced in the MAD-X file by drifts and kicks. This can be done with a MAKETHIN command, all elements which are called here get split into a number of thin slices which can be chosen by the user. Typically it is enough to split the elements in slices which represents a length of five to ten centimetre, but it has to be ensured that the Twiss parameters do not change much from the values of thick-lenses, to get reasonable results from the tracking. After slicing, a novel MATCH command should be done to calculate the new quadrupole strengths, which will have changed by the MAKETHIN command, to make sure that the optics properties are the same.

The fort.3 file include the input parameters with which SixTrack does the calculations. It is build-on blocks which are called by default keywords. They contain different characteristics of the tracking. For example in the TRAC block the number of turns and of pairs can be defined. Moreover, the beam energy and the emittance have to be specified in this file. For more information about all the parameters and conditions contained in fort.3 see the SixTrack User's Manual [11].
For the extended version of the code a new command block COLL is added to the fort.3 file, which contains the conditions of the collimation. Here the number of particle arrays and the initial distribution of them can be set, for detailed information of all additional options the homepage of this version is available at [12].

4.2 Target implementation

The target model described in chapter 3 has to be implemented in the tracking code. To simplify the use of the target in the code it is defined as a default collimator in the MAD-X sequence file, with zero length and unlimited horizontal and vertical half-apertures. In this way SixTrack treats the target as such an collimator and calls the additional subroutines available in the collimators version. The letters with which the name of the target-element have to begin is specified to "TARGET" or "target", otherwise it won't be identified as the right element and the novel target subroutine won't be called. This keyword is added to the other collimator names which are allowed. Now it is easy to call the target model out of an external file by adding an extra if-statement

at the right place in the collimation routine.

Only some minor corrections are left to be done in the model file. For the compability it is very important to ensure that the dimensions of the variables which are used in the model implementation are the same as in the collimation routine. Also the fact that the expanded version of SixTrack uses arrays with a length of 64 particles, causes a do-loop over one array around the main part of the target routine, since this routine is constructed for only one particle.

It could happen that the particles arrive with a too negative x-position and that they miss the target. Therefore they would not loose energy or do not get deviated. Consequently an additional if-statement should ensure that the target routine does not change any values in this case. Because of an negative wedge width the particle would otherwise increase its energy. This is an artefact of the formula implemented in the target routine.

To compare the particle distributions directly before and directly behinde the target an external file with the coordinates of the particles and their energies after each turn are written at these points. Moreover, we have to set a flag for every particle that it has hitten the collimator, otherwise the new particle coordinates after traversing the target are not taken into account.

4.3 Tracking

The purpose of a tracking is to calculate the trajectories of the particles to examine the blow up of the beam and there from the resulting particle losses. In that way we can understand and optimise the properties of the lattice, i.e. the strengths of the elements can be adjusted right and the particle loss can be studied and minimized.

As a first step of the tracking we concentrate on the target functionality and check if the target is working right inside the tracking code. A particle distribution is created at the beginning of the lattice, for this test the distribution "1" which is included in the collimation routine [12] is used. It creates only a flat distribution of particles which follows an ellipse in the phase space x-x' [15]. All particles are generated with a zero $\frac{\Delta p}{p}$, so that there is no spread in several ellipses, caused from a difference in the momentum, in the dispersion area of the target location. These are transferred through the first quarter of the ring, there they hits the target one time. To check the target behaviour two output files with the particle coordinates are written. One directly in front of the target and the other one directly behind it, after the first one forth of the first turn.
The comparison of this two distributions is shown in Fig. 4.1, the red dots are the coordinates of the particles before and the black ones are behind the target. As it is convenient to see, the particle get scattered by the target and the beam is blowed

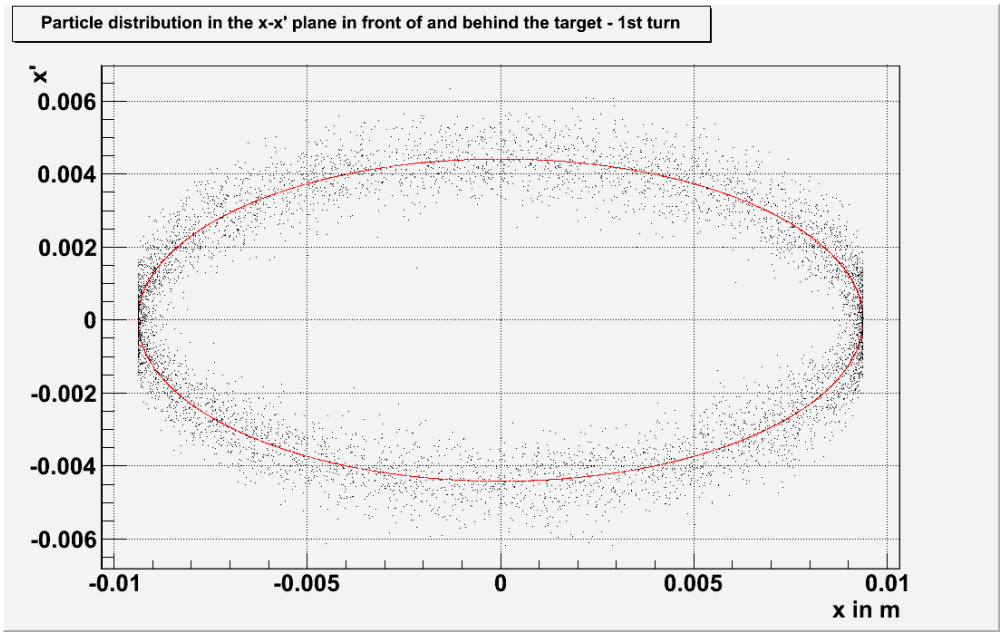

Figure 4.1: Comparison of the particle distribution in the x-x' plane directly before (red) and behind (black) the target after one fourth of the first turn.

up. The sharp cuts at the sides of the ellipse causes from the fact that the target only changes the x' coordinate of the particle, but not it's x coordinate. Therefore the ellipse does not increase in the x range and only in x'. Of course, the changes in angle will translate in change of position when the particles are transported through the elements of the ring. Theses examinations are also valid for the y-y' plane.

Figure 4.2 shows the outcome of our very first multi-pass simulations. Here the evolution in the x-x' phase space is plotted in six selected steps up to the first 100 truns. Therefore a superimposition of the first 2, 3, 5, 10 and 100 turns is shown, for comparison the distribution after the 1st turn is shown again. The red dots represent the particle coordinates directly before and the black ones behind the production target. One can see emittance blow-up and energy oscillation. The ellipse is moving because we are in a region of non-zero disperision, which leads to an additional x-offset of the beam and there from to a different energy loss in the target compared to a design particle.
To illustrate the dimension of the beam blow-up the last plot of Fig. 4.2 shows only the superimposition of the particle distributions behind the target after the first 100 turns (black) and in comparison to that the initial distribution (red) directly before the target, which is here exactly the same one as the red curve of the first plot.
Figure 4.3 shows the y-y' phase space. Here one only sees the beam-blow up, since in the vertical plane the dispersion is zero so it is not possible to see the energy oscillations.

In conclusion, for what concern the tracking, the tools has been put in place and preliminary multi-pass tracking simulations have been done. One should now create a more realistic particle distribution, which fits better to the real particle distribution expected after the injection into the production ring. A two dimensional Gaussian distribution in x-x', y-y' and in the longitudinal phase space has to be generated at the injection point.
We will then be ready to start simulations over several thousands of turns and study the evolution of the emittance in the three planes and start with the optimisation of the lattice, RF cavity and target in order to achieve some cooling in the three directions.

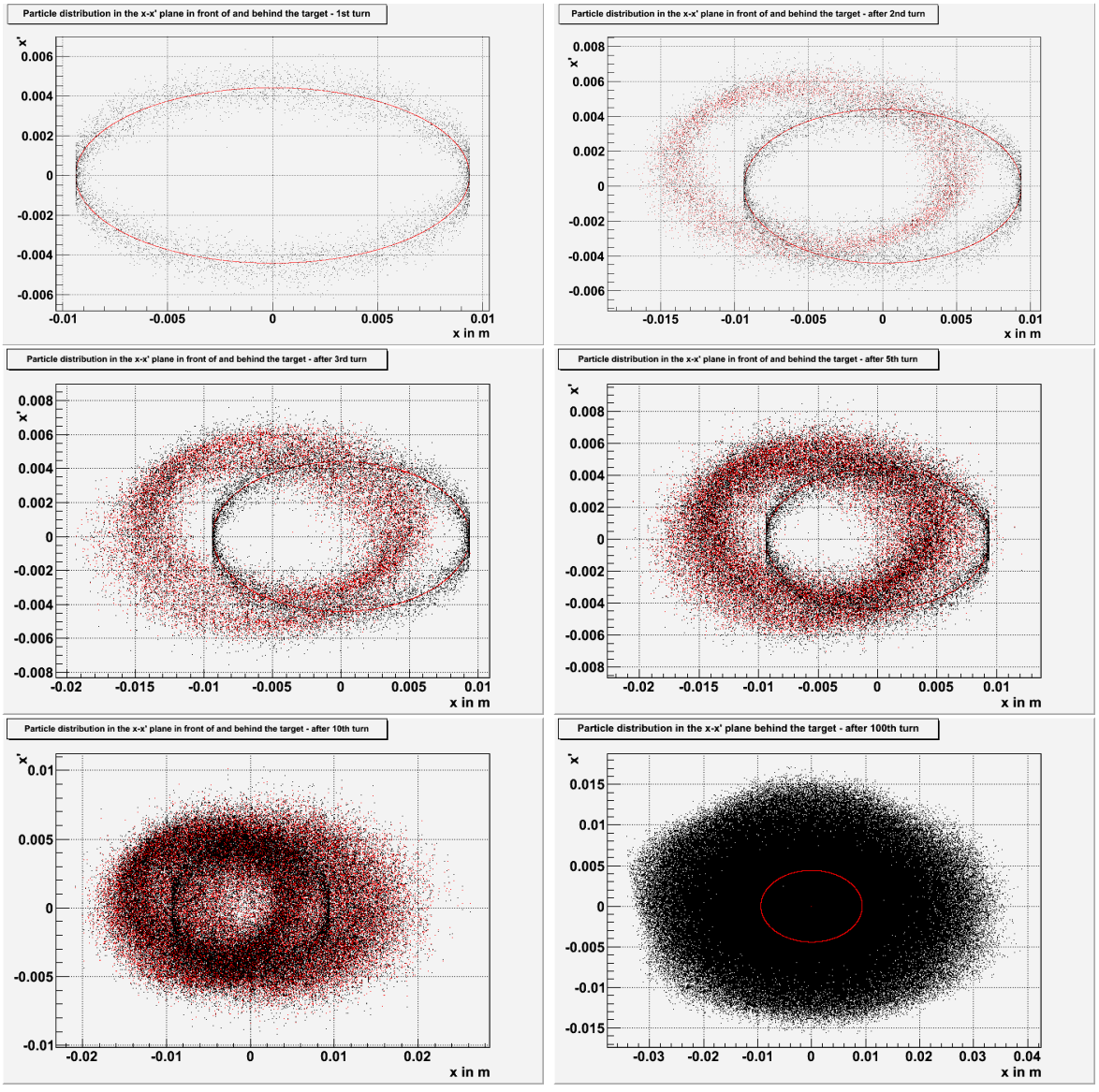

Figure 4.2: Multiturn tracking simulation in the x-x' phase space, particle distribution before (red) and behind the target (black) after the 1st, 2nd, 3rd, 5th, 10th and 100th turn.

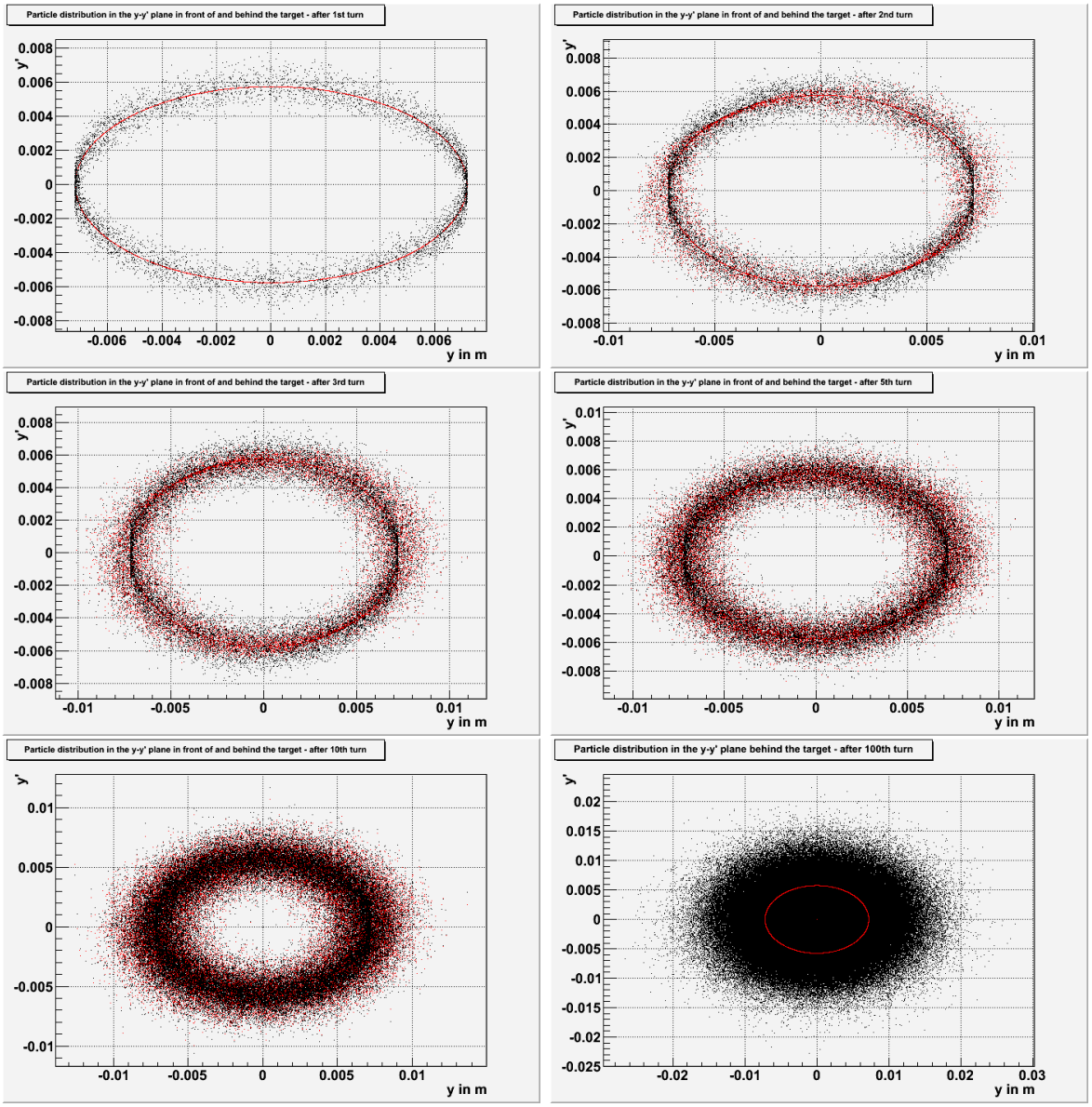

Figure 4.3: Multiturn tracking simulation in the y-y' phase space, particle distribution before (red) and behind the target (black) after the 1st, 2nd, 3rd, 5th, 10th and 100th turn.

5 Conclusion

A compact and flexible lattice design is developed based on the technique of the double bend achromat lattice. The layout includes five quadrupole families, three focusing and two defocusing, and two section dipole segments per cell. The ring is built of four cells, each $3\,m$ long which results in a circumference of $12\,m$. Moreover, the machine includes a two fold mirror symmetry which leads to high flexibility.
The geometry is such that there are four straight section of $80\,cm$ to install different equipments. Two of the straight sections have zero dispersion, in order to accommodate the RF cavities. The original design foresee the presence of only one cavity, but in principle it would be possible to add a second one, in case it is needed.
The other two straight section, instead, are characterized by a relatively high value of horizontal dispersion ($D_x \sim 50\,cm$), as required by the specifications for the production target, which will be installed in the middle of one of them.

The study includes a first evaluation of the required magnet aperture and the design is taking into account manufacture constrains. For sure, this first considerations need to be further optimised in respect to the compactness of the machine and, in particular once beam parameters such as the emittance and the momentum spread will be fully defined from injection and cooling constrains.
We will also have to study in more detail the quarter of the ring after the target and before the RF cavity, in which the particles will have a lower energy than the design one and may be lost in the bending magnets.

As it has been designed, the lattice is compact and flexible enough so that it will be easy to optimise it in the future, but it can already be used for preliminary tracking studies [3] and to start understanding the cooling processes.

In addition to the lattice design, the tracking tools have been put in place for future studies. A simplified target model has been implemented inside SixTrack, a fully 6D tracking code developed and widely used at CERN. A new subroutine is included in the code and is activated any time the particles encounter and element named with the keyword "TARGET", in analogy to what is done for the CERN Large Hadron Collider collimator studies.
Our simplified modelling of the production target takes into account the Coulomb scattering and the energy losses via analytical formula, such as Bethe-Bloch formula, which have been benchmarked with detailed Geant4 simulations [3] for the energy range of interest. This model only describes the target as a kick in the direction and the energy loss is calculated independently.

The basic check of functionality of the routine has been completed and preliminary multi-pass tracking simulations have been done, showing beam size blow-up in the transverse plane due to the scattering at the screen.

Within the context of this thesis a lattice for a very compact and still flexible storage ring design has been developed and optimised. All the tools for the further tracking simulations are prepared and first tests using these tools for particle tracking calculations have been performed.

Next steps will require a tracking campaign of a more realistic 6D particle distribution to see the evolution over several thousands of turns of the quantities of interests (emittances on the three planes, beam sizes and energy spread), in order to start the work of optimisation of target, RF cavities and lattice for an effective particle cooling in the three planes.

6 Acknowledgement

I appreciated the freedom I got from my supervisor Achim Stahl and Elena Wildner, who supervised my project at CERN, as it enabled me to collaborate with many different scientists and aided in shaping my selfmotivation and independence. I am also grateful to her for hosting me during the three month of my stay at CERN.
Due to the financial support form the FP6 "Structuring the European Research Area" programme, "CARE", contract number RII3-CT-2003-506395 and FP7 "Capacities Specific Programme, Research infrastructures", "EUROnu", Grant agreement number 212372 my stay at CERN for preparing this thesis was enabeled.
I am deeply indebted to Bernhardt Holzer for all the time and effort he has spent in our discussions, I learned a lot. You were a great help, thank you very much.
I would like to thank Elena Benedetto, who contributed significantly to my work. She supports my ideas and always tried to help solving several problems.
Several people were helpful in shaping this manuscript. I would like to express thanks to Chiara Bracco, Valentina Previtali and Frank Schmidt, who helped me with the simulations with SixTrack. Also I would like to thank Christian Hansen.

Last but not least I would like to thank Markus Zimmermann, not directly involved in the creation of the thesis, for the mental support. You have always been there for me.

Many thanks to all of you, it was a nice time and a great experience to work with you.

Bibliography

[1] C. Rubbia, A. Ferrari, Y. Kadi and V. Vlachoudis *Beam Cooling with ionisation losses,* Nucl. Inst. and Meth. A568 (2006) 475-487

[2] David Neuffer *Low-energy ionization cooling of ions for beta beam sources,* Nucl. Inst. and Meth. A585 (2008) 109-116

[3] Jakob Wehner *Monte Carlo simulation of an ion-production ring for a beta beam neutrino facility*

[4] MAD-X User's Manual *http://mad.web.cern.ch/mad/*

[5] CAS CERN Accelerator School *fifth gerneral accelerator physics course* proceedings CERN 94-01

[6] CAS CERN Accelerator School *Intermediate accelerator physics* proceedings CERN 2006-002

[7] CAS CERN Accelerator School *Synchrotron radiation and free electron lasers* CERN-98-04

[8] K. Wille *Physik der Teilchenbeschleuniger und Synchrotronstrahlungsquellen*

[9] Helmut Wiedemann *Particle Accelerator Physics* Basic Principles and Linear Beam Dynamics

[10] PDG *Particle Data Booklet, http://pdg.lbl.gov/*

[11] SixTrack User's Reference Manuel *Single Particle Tracking Code Treating Transverse Motion with Synchrotron Oscillations in Symplectic Manner,* CERN-SL-94-56-AP, Update July 2008

[12] Extended version of SixTrack for collimators *http://lhc-collimation-project.web.cern.ch/lhc-collimation-project/code-tracking.htm*

[13] Valentina Previtali *Private comunication*

[14] Chiara Bracco *Private comunication*

[15] Chiara Bracco *Commissioning Scenarios and Tests for the LHC Collimation system,* CERN-THESIS-2009-031

[16] Elena Wildner *New Opportunities in the Physics Landscape at CERN: Beta Beams ion production http://indico.cern.ch/conferenceOtherViews.py?view=standard&confId=51128*